Hindawi
Wireless Communications and Mobile Computing
Volume 2020, Article ID 9578031, 14 pages
https://doi.org/10.1155/2020/9578031

Research Article

Development of Multilayer Partially Reflective Surfaces for Highly Directive Cavity Antennas: A Study

Sapna B. Abdulkareem and Srivatsun Gopalakrishnan

Department of Electronics and Communication Engineering, PSG College of Technology, Coimbatore 641004, Tamil Nadu, India

Correspondence should be addressed to Sapna B. Abdulkareem; sapna.psmi@gmail.com

Received 12 September 2019; Revised 28 November 2019; Accepted 19 December 2019; Published 22 January 2020

Academic Editor: Petros Nicopolitidis

This paper proposes a novel triple-layer partially reflecting surface (PRS) for designing a highly directive antenna. The proposed PRS design has 54% improvement in impedance bandwidth with existing design. The design has multiple cavities, optimized for improved gain and bandwidth performance. The PRS arrays are printed on the dielectric substrate, placed above the ground plane at a height of approximately half wavelength. The reference square microstrip patch antenna operating at a frequency of 5.8 GHz with a gain of 3.77 dBi is enhanced to 13.54 dBi. The measured S_{11} of the fabricated prototype is −22.12 dB with a VSWR of 1.17 : 1. Measured 3 dB gain bandwidth of the antenna is 390 MHz which is an improvement of 50% compared with the reference antenna. This highly directive antenna is suitable for WiMAX wireless application.

1. Introduction

The Fabry–Perot cavity (FPC) leaky wave antennas have been explored as a promising design solution to realize highly efficient radiators. Conventional high-gain aperture antennas like huge reflectors and large array structures are replaced by a simple, compact, and low profile PRS superstrate antennas. FPC antennas are designed with a ground plane, a reflector, and a radiator. The reflectors are normally periodic in nature with 1D, 2D, or 3D metallic conductors or apertures in a metallic sheet capable of partially reflecting and transmitting the incident signals. They are separated from the ground plane by half a wavelength enabling in phase radiation of reflected signals. Low-gain antennas like dipole, slot, or microstrips can act as the radiating sources. The restricted bandwidth of resonant cavities limits them to be operational with reduced bandwidth [1, 2]. Several works have been reported to improve the bandwidth and maintain high gain at upper frequency wireless spectrum [3–8]. Single- and dual-layer high-gain FPC antennas are studied in the literature [9–11]. The leaky wave nature of the PRS-FPC antenna is explained in [12]. Multilayer PRS broadband and high-gain antennas are analysed by Konstantinidis et al. and Mohammed Aymen et al. [13–15]. High-gain single-layer and multilayer antennas with different feed radiators and polarizations are analysed [8, 16–29]. The FPC antennas find wide applications in modern wireless communication, in radars (RCS reduction), and in networking sectors [30–32]. They are also employable in cognitive application for beam scanning, with reconfigurable designs using microelectromechanical switches (MEMS) and active elements [33–35]. FPC antennas are also employed in UWB applications [36, 37].

This paper gives an insight of theory and working of the PRS antenna followed by the design and analysis of a proposed multilayer PRS antenna for gain enhancement. The reflecting structure configuration is studied and optimized to have maximum phase reflection characteristics with increase in frequency. Presence of two cavities due to the PRS layers of different designs exhibits dual resonances. The high-gain prototype antenna is tested and measured to validate the experimental and simulated results.

The advent of partially reflecting sheets in antennas by Trentini [1] paves the way to use a simple technique to improve the gain and the directivity of conventional antennas like monopole and microstrip patch antennas. PRS

structures are simple metallic arrays printable on dielectric substrates with partially reflecting property following ray optic theory. Figure 1 depicts the schematic model and the concept of a typical FPC cavity antenna. It consists of a source radiator, a PEC (perfect electric conductor) ground plane, and a PRS layer of multiple reflective cells. The electromagnetic wave radiated from the source antenna is partially reflected through the PRS layer. A portion of the radiated signal which reflects from the PRS strikes off the ground plane and bounces back to PRS where it again transmits partially. If the ground and PRS planes are infinite in nature, this process repeats indefinitely. If the distance between the layers is properly fixed, reflected beams contribute to form a pencil beam radiation pattern thus achieving high-gain antennas.

According to the theory [1], a pattern maxima can be observed at bore sight ($\theta = 0^{\circ}$) if the phase satisfies the condition

$$\psi_R - \pi - \frac{4\pi h \cos\theta}{\lambda} = 2N\pi, \quad \text{for } N = 0, 1, 2, \ldots. \tag{1}$$

Typical reflection phase of PRS ψ_R at zero degree is close to $-\pi$ making the practical height h between the PRS and the PEC ground to be approximately half wavelength. Analysis of equation (1) concludes that the height obtained with different N values may not be practically feasible and the phase condition is satisfied only at the designed frequency.

The paper is organised as follows. Section 1 introduces a novel multilayer PRS antenna. Section 2 analyses the different unit cell PRS topologies with design specifications. Section 3 discusses the fabricated cavity antenna. Section 4 shows the analysis of the measured results. Finally, Section 5 concludes with the findings and summary of the research.

2. Topology of the PRS Unit Cell

Initially, a single-layer novel PRS unit cell structure has been designed and is then modified to form a triple-layer PRS unit cell. The three layers of PRS unit cells are printed on a commercially available 1.6 mm thick FR-4 glass epoxy substrate with a dielectric permittivity (ε) of 4.3 and a loss tangent (δ) of 0.025. The thickness of the conductor is 0.035 mm. The proposed single-layer PRS unit cell (PRS1) with dimensions is shown in Figure 2(a). The design structure consists of an inner metallic square and an outer loop with two slots, appearing as alphabet "*E*." The inner square section and the outer loop are bridged with the smaller strip of "*E*" whose length is equal to the width of the loop. The designed unit cell structure has a periodicity (P) of 14.56 mm. Figure 2(c) shows the cross-sectional view of the proposed triple-layer PRS unit cell. It is constructed with two layers of the designed PRS1 unit cells on top and bottom. The middle layer is of PRS design 2 (PRS2) as in Figure 2(b), which consists of an inner square and an outer loop adopted from [6] with a change in dimension, scaled, and optimized to 5.8 GHz maintaining the same periodicity of 14.56 mm. The layouts of the two PRS designs with specifications are shown in Figure 2, and their parametric dimensions are tabulated in Table 1.

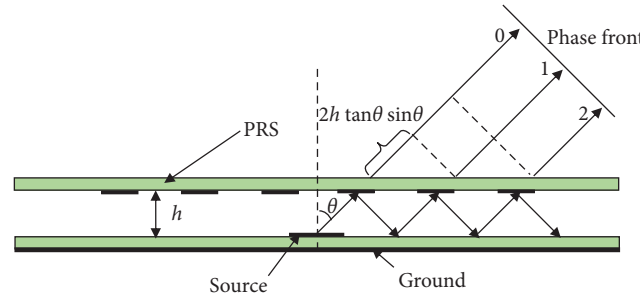

Figure 1: Schematic of a typical PRS Fabry–Perot cavity antenna.

The two PRS structures are optimized to have good reflectivity characteristics. Simulations are carried out using CST Microwave Studio by setting periodic unit cell boundary conditions. Perfect electric (E) and magnetic (H) boundary walls are provided in "x" and "y" directions, and a plane wave excitation is incident on the PRS layer along "z" direction. The reflection phase characteristic for single-, dual-, and triple-layer PRS unit cells with different combinations is analysed. Periodicity and dimensions of the unit cell are optimized to achieve a positive gradient of reflection phase characteristics. The size of the single-layer unit cell has a square dimension of $0.28\lambda \times 0.28\lambda$ at the operating frequency of 5.8 GHz. The dual-layer PRS consists of PRS1 and PRS2 layers separated by an optimal height of $h_1 = 32.1$ mm. The designed triple-layer PRS has an optimal lower and upper cavity heights of $h_1 = 32.1$ mm and $h_2 = 30$ mm, respectively.

Figures 3(a) and 3(b) exhibit the complex reflection characteristic of PRS unit cells with frequency along the x-axis and the magnitude and phase along the y-axis. The single-layer PRS unit cell achieves a minimum value of reflection magnitude −33.23 dB at 5.8 GHz with a phase transition from −180° to +180°. The phase transition indicates the reflecting nature of the PRS cell. Single-layer PRS has a larger bandwidth of 1.27 GHz ranging from 5.46 GHz to 6.73 GHz. It can be observed that there are two minima in the reflection magnitude curves of dual- and triple-layer PRS compared with the single-layer PRS. The two resonances of dual-layer PRS occur at 4.56 GHz and 5.8 GHz, respectively. A larger band of 891 MHz is obtained at the second band ranging from 5.569 GHz to 6.46 GHz. The phase curves show multiple transitions confirming the dual-band operation. The first band is narrow with only 60 MHz, and the phase transition is from −55° to 85°. For the proposed triple-layer PRS unit cell, zero reflection phases are achieved at two resonances by adjusting the cavity heights. The plots show the lowest reflection magnitudes as −22.815 dB and −36.1 dB corresponding to the resonant frequencies 4.52 GHz and 5.8 GHz. The phase varies from −180° to +180° leading to a bandwidth of 780 MHz in the upper band and 50 MHz in the lower band. In Figure 3(c), the reflection magnitude of the proposed novel unit cell design structure (PRS1) is compared with the existing design (PRS2). The existing unit cell design has a bandwidth of 670 MHz, while the proposed design has increased bandwidth of 1.24 GHz, which is an improvement of 54%. Improvement in the bandwidth of the

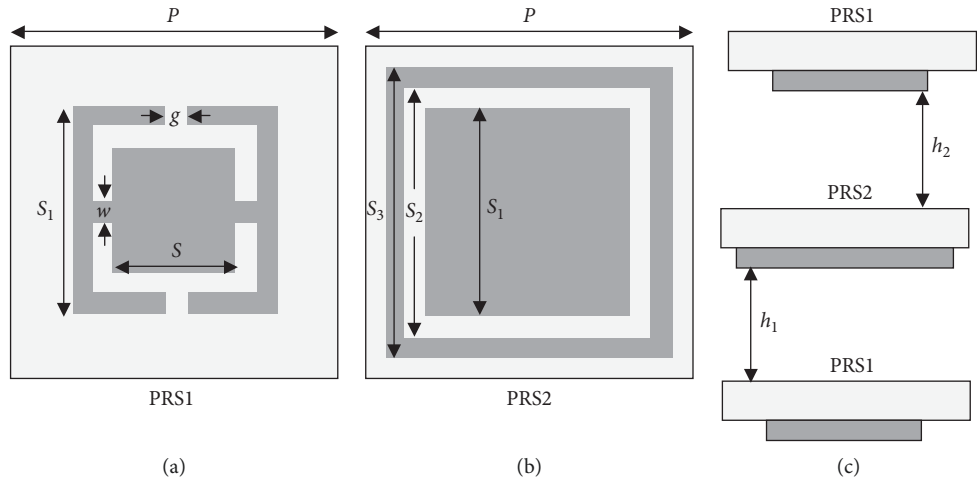

Figure 2: Layout designs of the PRS unit cell: (a) design of the top and bottom layer—PRS1; (b) design of the middle layer—PRS2; (c) schematic of the triple-layer PRS unit cell.

Table 1: Specifications of the PRS unit cells.

Parameter		Dimensions (mm)
Periodicity	P	14.56
Inner square side of PRS1	S	4.56
Sides of outer loop of PRS1 and inner square of PRS2	S_1	8.56
Slot length of PRS2	S_2	10.56
Loop length of PRS2	S_3	13.56
Slot gap	g	1
Strip width	w	1
Lower cavity height	h_1	32.1
Upper cavity height	h_2	30

PRS cell would enhance antenna performance in terms of bandwidth and directivity when placed above the reference source antenna.

3. Design of the Cavity Antenna

The prototype of the proposed triple-layer PRS cavity antenna is fabricated, and the measured results are validated with the simulated results. The photograph of the printed PRS layers and the assembled antenna is portrayed in Figure 4. The source radiator shown in Figure 4(a) is a conventional square microstrip patch antenna with side length 12.26 mm and operating at a frequency of 5.8 GHz. This source antenna is considered as the reference antenna for analysis.

The PRS layers are formed by a 5×5 array of the optimized triple-layer PRS unit cell. Figure 4(b) represents the triple-layer PRS antenna. The two PRS layers with designs PRS1 and PRS2 are shown in Figures 4(c) and 4(d), respectively. The size of the PRS array is 72.8 mm $\times$ 72.8 mm. The heights of the PRS layers above the ground plane are optimized to achieve maximum gain and operational bandwidth. The optimized cavity height of the single-layer PRS antenna is 29.5 mm. Maximum gain for the dual-layer antenna is achieved with h_1 and h_2, respectively, at 30 mm and 13 mm. In the triple-layer PRS antenna, the cavity height between the source antenna and the first PRS layer is 30 mm and between two upper PRS layers is13 mm and 29 mm, respectively, making the antenna height as 1.48λ. Bearing the practicality of fabrication, the dimensions of the antenna are slightly increased along the length and width. The fabricated antenna has a total measured measure of 85 mm $\times$ 125 mm. The prototype with multilayer PRS is assembled with plastic spacers between the layers.

4. Results and Discussion

The antenna parameters, like return loss, VSWR, and gain, are simulated using electromagnetic simulation software. The designed reference patch antenna is simulated to obtain optimal characteristics to match the design of PRS array combinations. Reflection and radiation characteristics of the designed patch antenna at 5.8 GHz are analysed and optimized with the feed and ground plane variations to have matched resonance with good return loss. Ground plane is varied from 1.4λ to 1.9λ, and the results are plotted in Figure 5(a). The maximum return loss is obtained for 1.42λ, but there is a left shift in the resonant frequency. The simulation results show a return loss of 32.59 dB at 5.8 GHz for the ground size of 1.65λ. The plots in Figure 5(b) show the gain of the patch antenna with the variations in ground plane size, and the obtained gain varies from 3.3 dB to 4 dB. The maximum gain of 4 dB is obtained for the ground size of 1.42λ corresponding to a frequency of 5.6 GHz. At 5.8 GHz, the maximum gain is 3.9 dB for the ground size of 1.65λ. The larger ground size of 1.89λ resulted in the minimum gain value of 3.3 dB at 5.8 GHz. With the results of Figures 5(a) and 5(b), the patch antenna with a ground size of 1.65λ with good return loss and maximum gain at 5.8 GHz is chosen as the reference antenna for further analysis.

4.1. Reflection Characteristics of the PRS Antenna. The reflection parameters of the antenna, like return loss and the

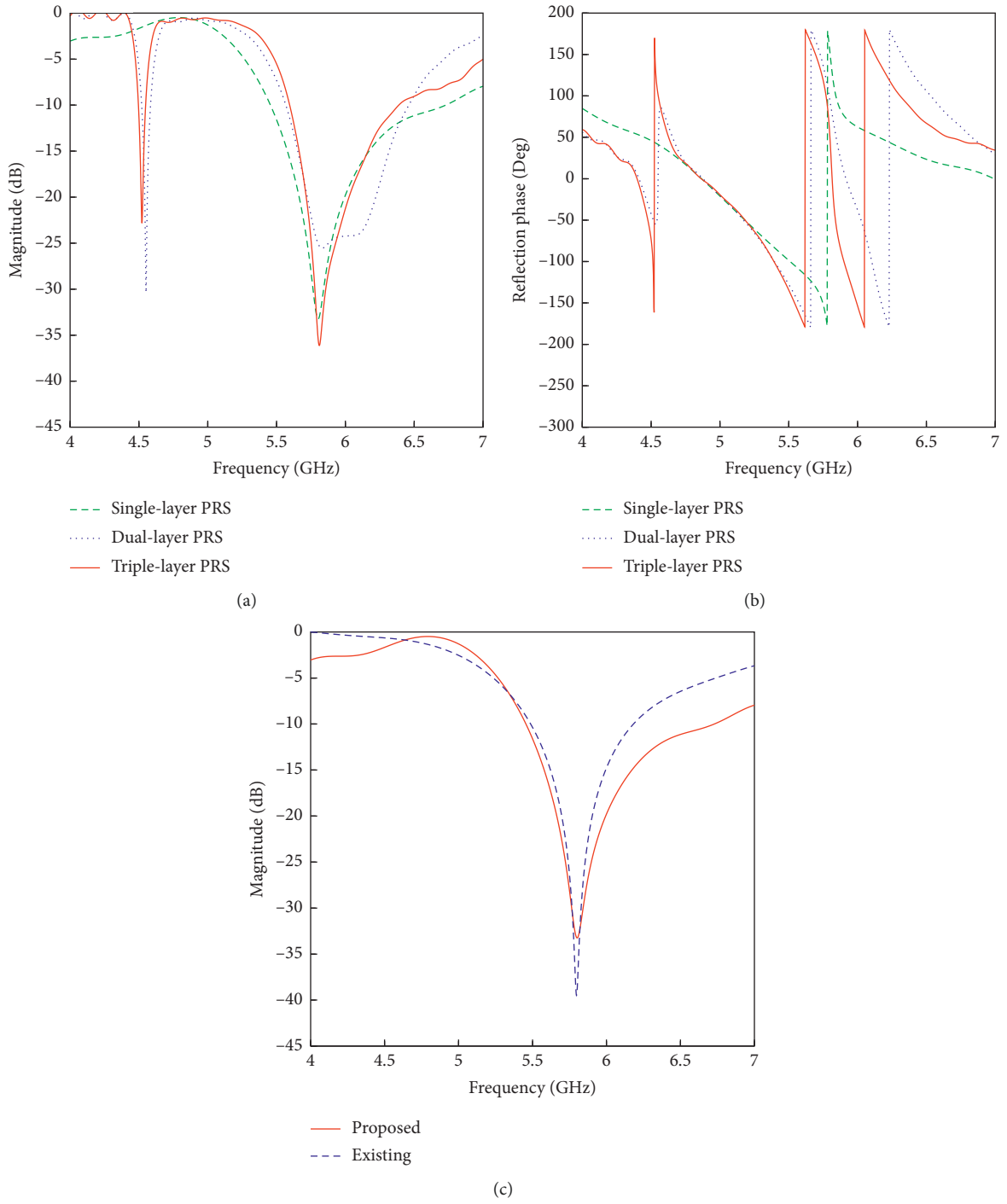

FIGURE 3: Reflection characteristics of the PRS unit cells: (a) reflection magnitude; (b) reflection phase; (c) reflection magnitude comparison of existing and proposed unit cell design.

VSWR, are measured with Agilent Vector Network Analyser to validate the simulated results. During simulation, different square array PRS combinations with 4×4, 5×5, and 6×6 elements were configured to analyse the performance of the designed antenna. In order to improve the gain performance of the antenna, the reflecting layers of different designs were arranged in multiple stacks in the vertical direction. Optimized reflection characteristics of the cavity antenna with single, dual, and triple PRS layer for different array sizes having 4×4, 5×5, and 6×6 elements are shown in Figure 6. Ground size of the antenna is maintained constant at 1.65λ. Analysis of Figures 6(a)–6(c) shows that the return loss plot of the 5×5 element triple-layer PRS antenna has maximum impedance

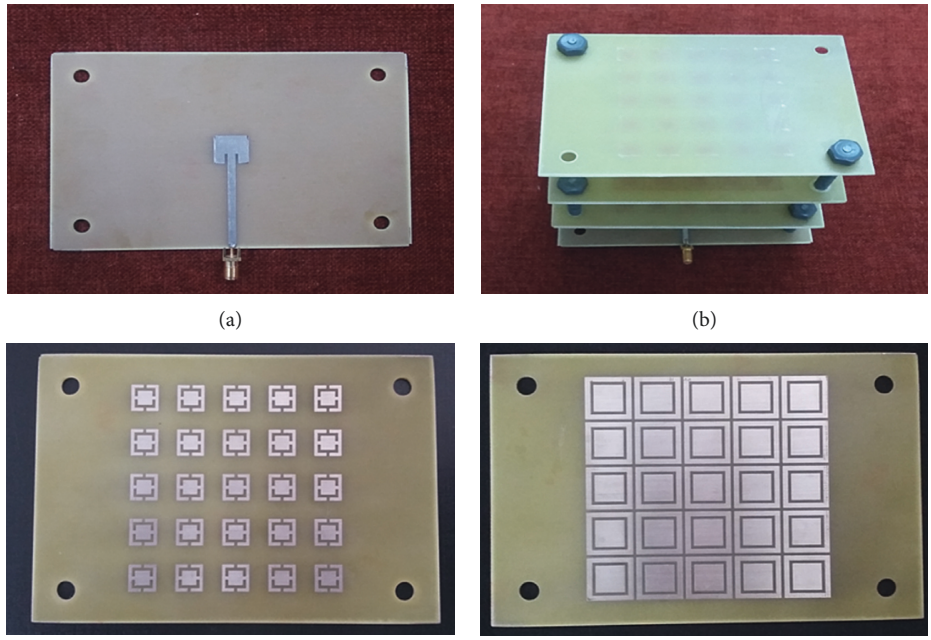

FIGURE 4: Photograph of the fabricated antenna: (a) reference antenna; (b) triple-layer PRS antenna; (c) printed top and bottom PRS layer design (PRS1); (d) printed middle-layer PRS design (PRS2).

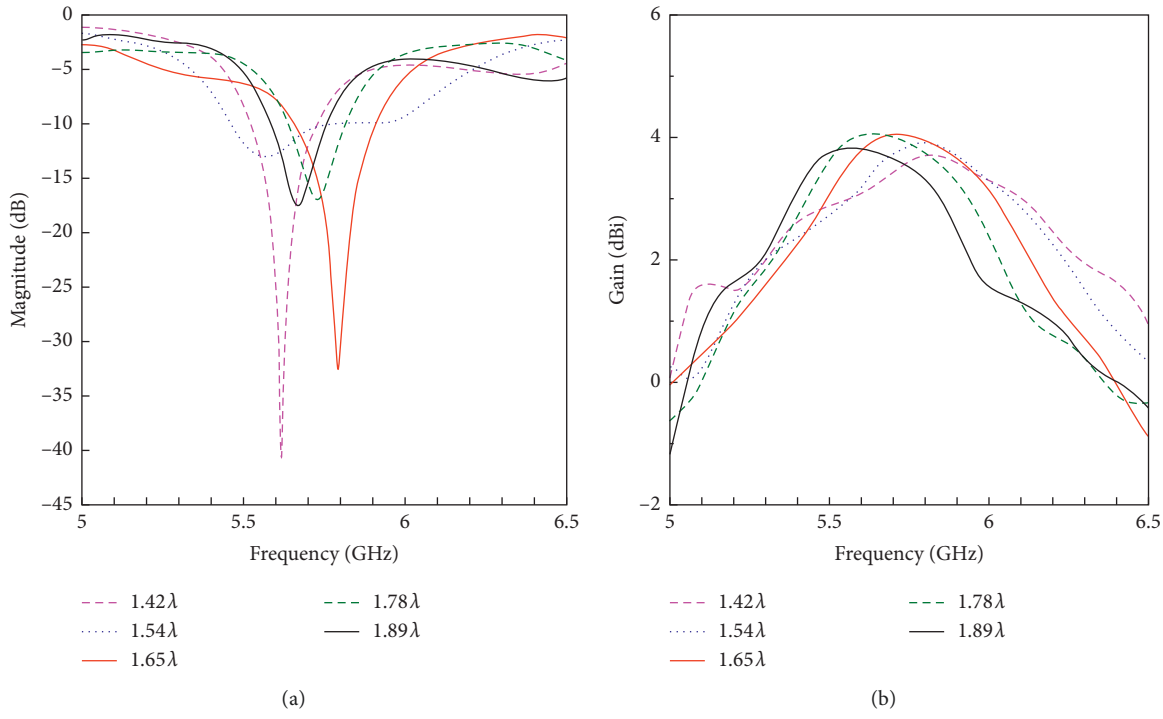

FIGURE 5: Parametric optimization of the reference antenna with respect to ground size: (a) return loss and (b) gain.

bandwidth 360 MHz ranging from 5.624 GHz to 5.984 GHz. Figures 7(a)–7(c) indicate the VSWR plots for the single-layer, dual-layer, and triple-layer PRS antenna for different PRS array combinations are within the acceptable limit of less than two. Return loss and VSWR plots show that the PRS array of 5×5 elements with the triple-layer PRS antenna is the best out of all other configurations.

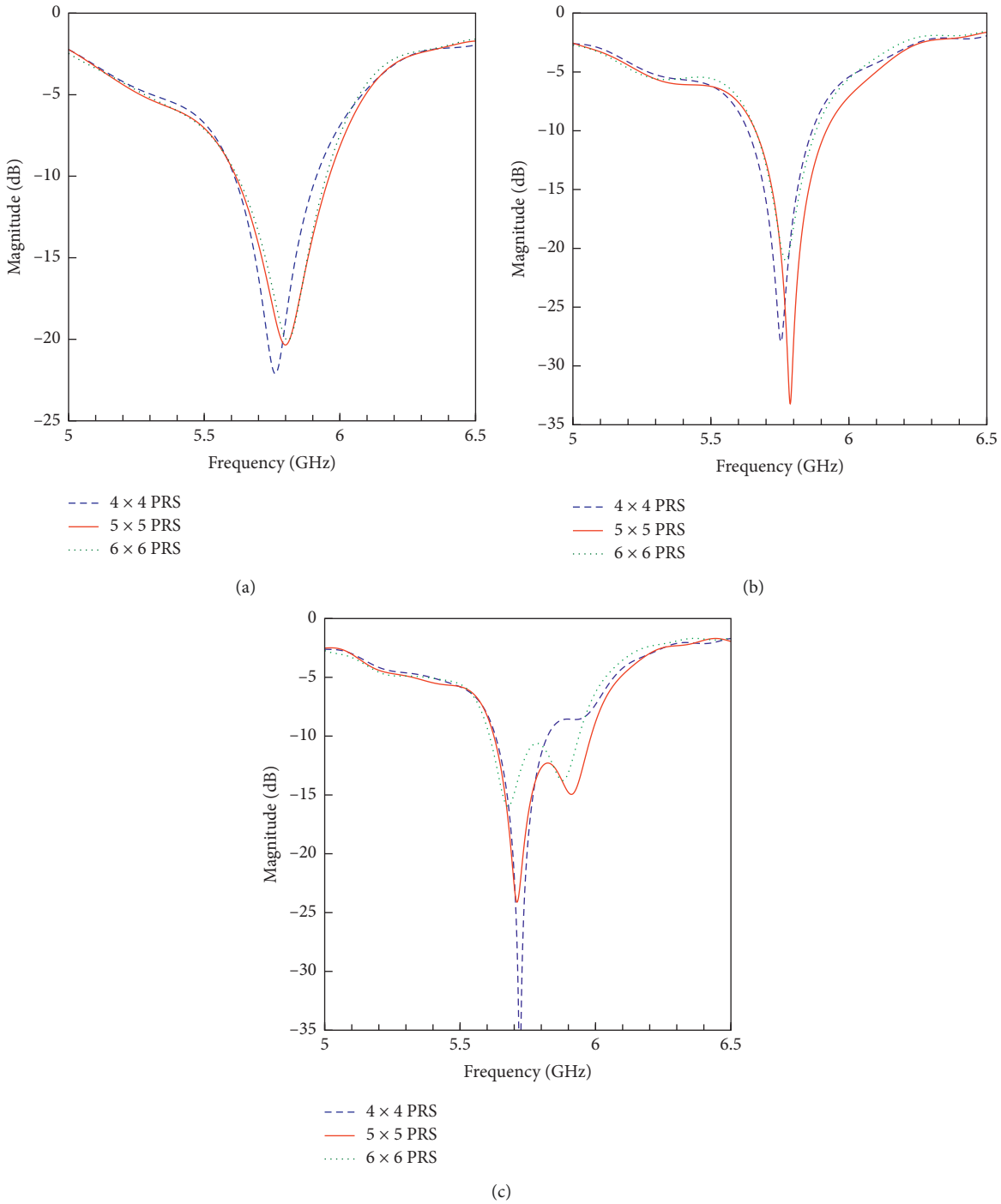

Figure 6: Simulated return loss of the PRS antenna with respect to array size: (a) single layer, (b) dual layer, and (c) triple layer.

Figures 8(a) and 8(b) represent the measured and simulated return loss and VSWR of the fabricated PRS antennas with reference to the source antenna. With reference to $S_{11} < -10$ dB, all antenna configurations of the 5×5 PRS array have good impedance matching at 5.8 GHz. Triple-layer PRS antenna measures a return loss of 22.12 dB with VSWR of 1.17 : 1 at 5.72 GHz. These measured results are in proximity to simulated return loss of 24.08 dB and VSWR of 1.13 : 1.

4.2. Radiation Characteristics. The field patterns of the antenna are measured against a single ridged-horn antenna with a standard gain and operational in the frequency range

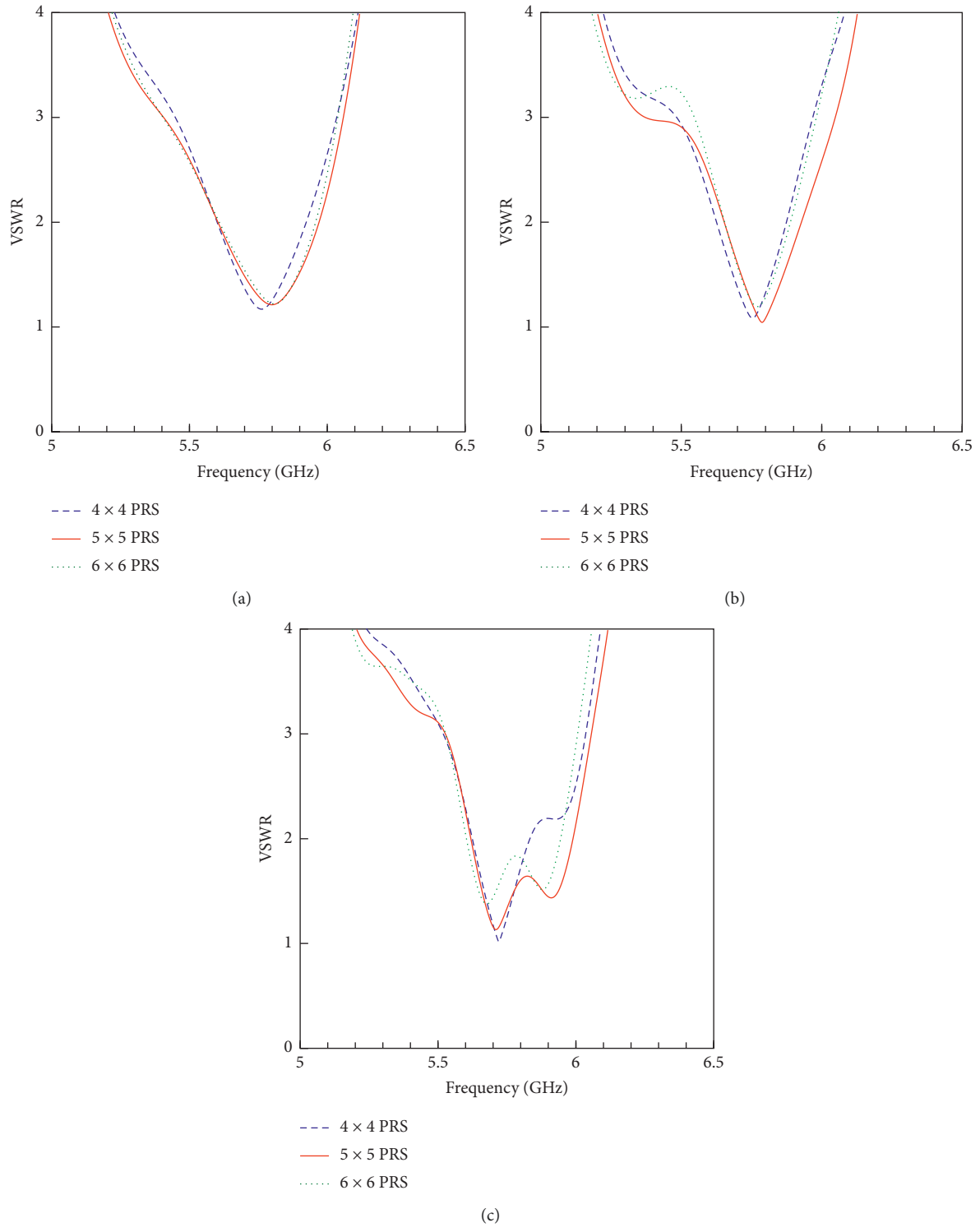

Figure 7: Simulated VSWR of the PRS antenna with respect to array size: (a) single layer, (b) dual layer, and (c) triple layer.

of 1–12 GHz. The measurements are carried out in an anechoic chamber. The distance of separation between the reference antenna and the test antenna is maintained larger than $2D^2/\lambda$, where D is the largest dimension of the antenna. The electric and magnetic fields are measured separately by fixing the standard reference antenna in horizontal and vertical directions, thereby changing the polarization.

Radiation patterns of 5×5 array PRS antennas are analysed for varied ground size. Figures 9(a) and 9(b) show

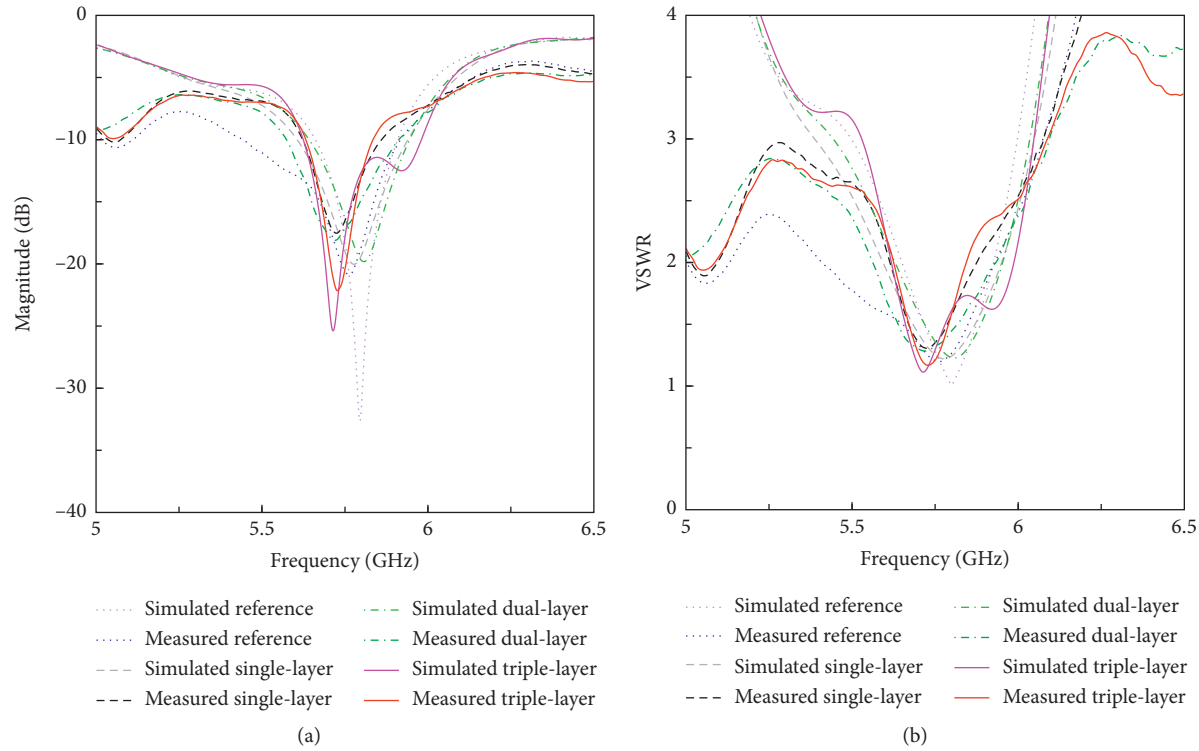

Figure 8: Measured and simulated reflection characteristics of proposed PRS antennas: (a) return loss and (b) VSWR.

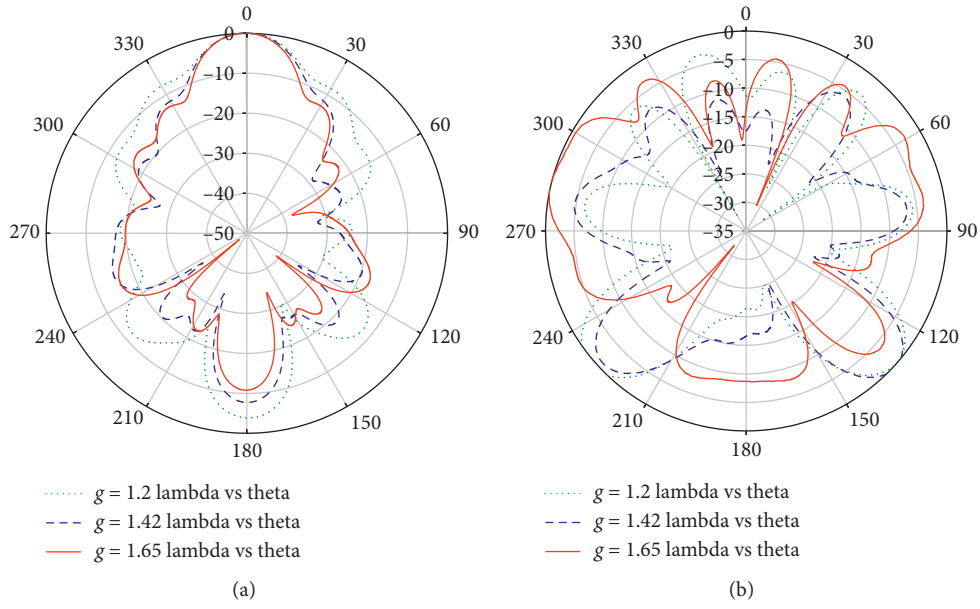

Figure 9: Simulated radiation patterns of the 5 × 5 PRS antenna with varying ground plane: (a) *E*-plane radiation patterns; (b) *H*-plane radiation patterns.

the simulated electric and magnetic field radiation patterns of the proposed PRS antenna with ground sizes of 1.2λ, 1.42λ, and, 1.65λ. Antenna with smaller ground has a wider main lobe and lower magnitude compared with the larger ground antenna. The size of the ground plane reflects the back radiations, thus increasing the antenna gain. Considering the return loss, the antenna with lower ground plane deviates from the resonance frequency, so the antenna with a ground size of 1.65λ having good impedance match is chosen for fabrication. Simulations are performed for

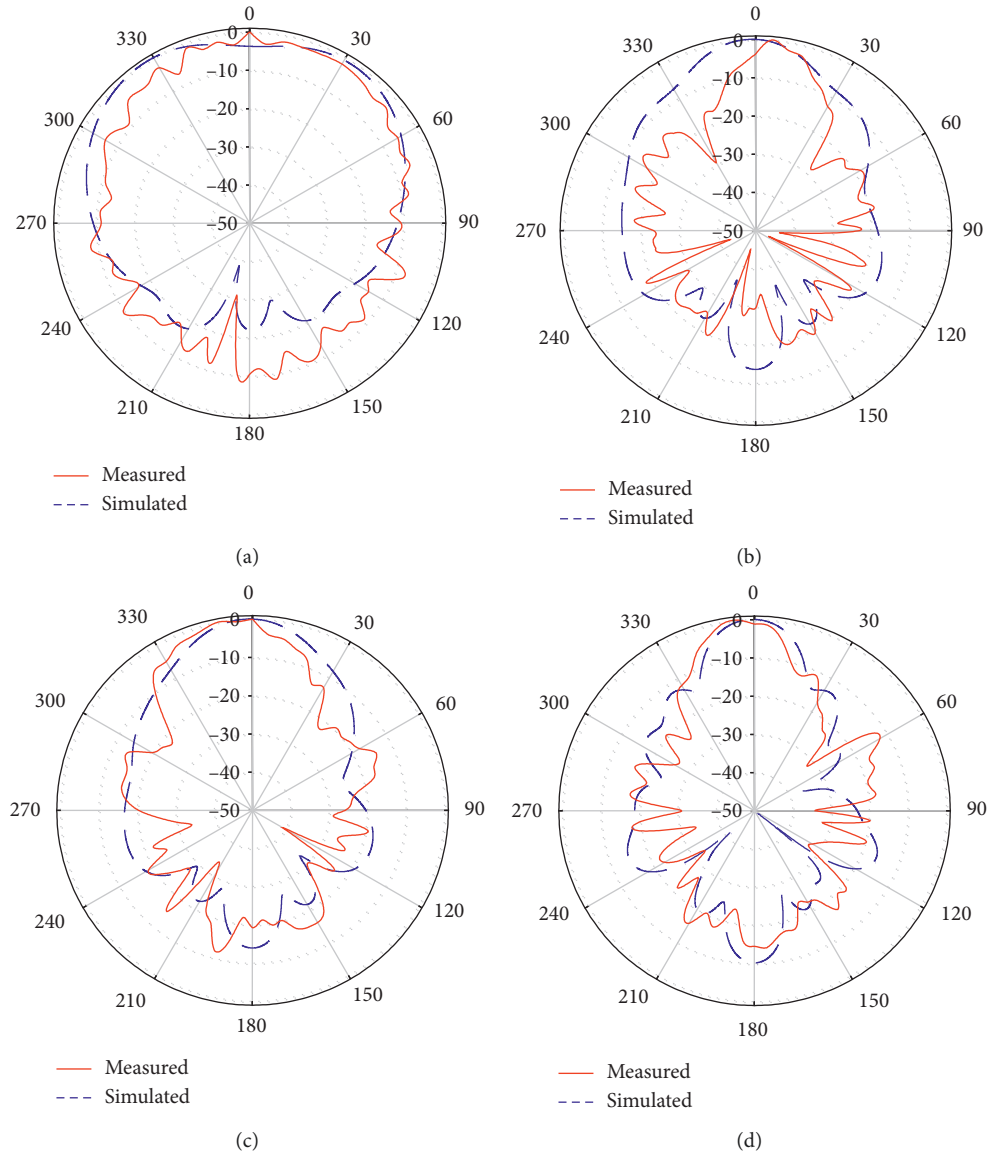

Figure 10: Simulated and measured E-field radiation patterns of the antennas: (a) reference antenna; (b) single-layer PRS antenna; (c) dual-layer PRS antenna; (d) triple-layer PRS antenna.

single-, dual-, and triple-layer PRS antennas with 5×5 element reflecting surface. Measured and simulated performance comparison of normalized electric and magnetic field patterns for different antenna configurations is plotted in Figures 10 and 11. The E-field radiation patterns in Figures 10(a)–10(d) clearly indicate that the patterns are more directive at bore sight, proportionately with an increase in the cavities and reflective layers.

In the measured result of single-layer PRS antennas, the maxima of E-field have a slight shift from zero axis. The measured E-field patterns of double- and triple-layer PRS antennas are similar to the simulated E-field patterns, with a maximum value for the triple-layer PRS antenna. The reference antenna has a 3 dB beamwidth of 53 degrees, while the triple-layer PRS antenna has a narrow beam of 22 degrees. Triple-layer PRS antenna has the highest main lobe magnitude of 13.7 dB. The measured H-field patterns depicted in Figures 11(a) through 11(d) show near omnidirectional pattern for all four cases with variations in magnitude. The variations in the envelope of the H-plane pattern attribute to the lossy nature of the material. During simulation, double- and triple-layer PRS antennas follow similar H-field patterns, while the reference and single-layer PRS antenna have related patterns. The simulated E- and H-field radiation patterns have a smooth edge, while the measured radiation patterns follow a zigzag uneven edge with lower magnitudes.

The measured and simulated gain comparison of various PRS antenna configurations is plotted in Figure 12. Simulated results of Figures 12(a)–12(c) show that

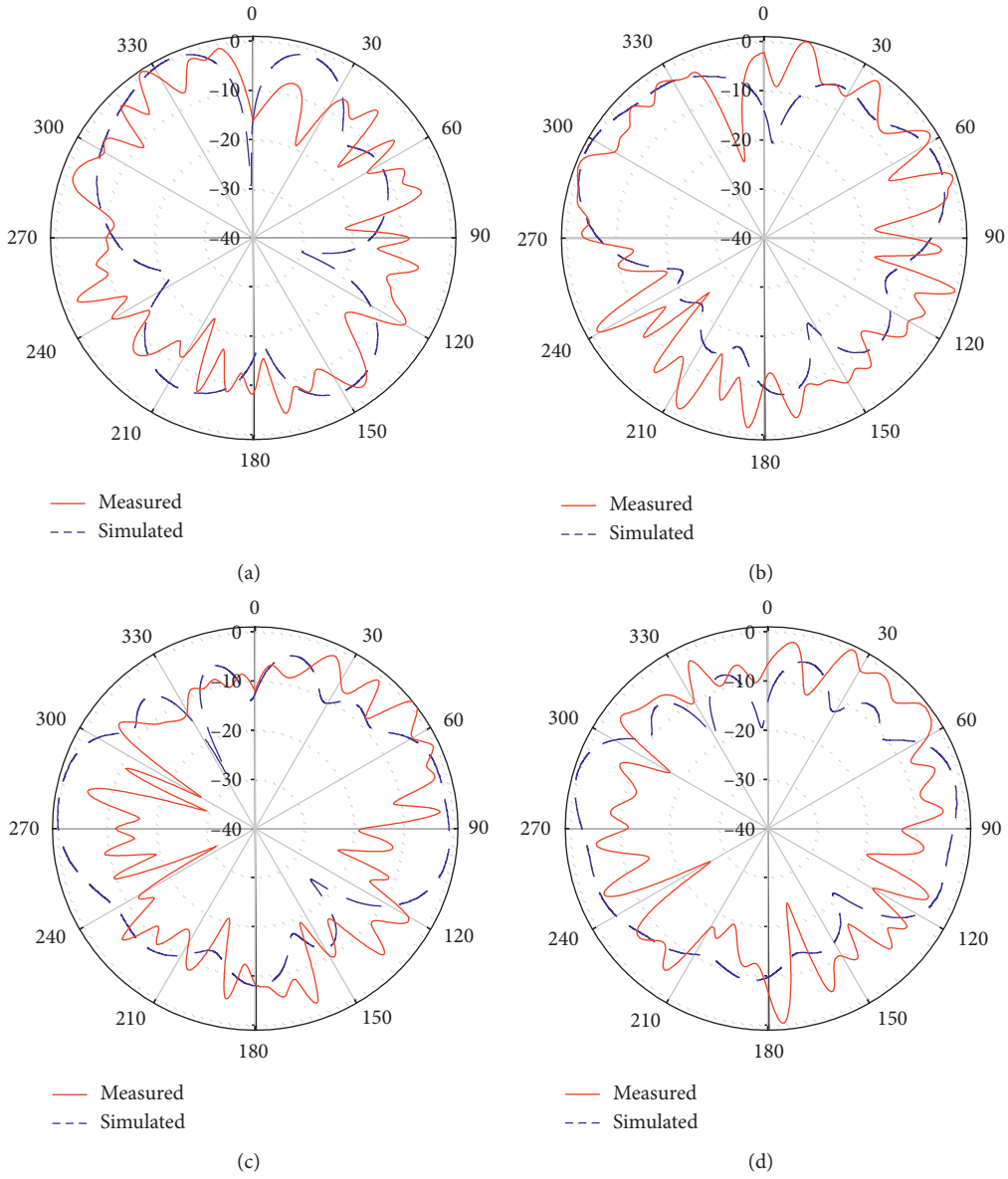

Figure 11: Simulated and measured H-field radiation patterns of the antennas: (a) reference antenna; (b) single-layer PRS antenna; (c) dual-layer PRS antenna; (d) triple-layer PRS antenna.

5×5 array antennas have higher gain compared with 4×4 and 6×6 arrays at 5.8 GHz. Measured 3 dB gain bandwidth of the reference antenna is 180 MHz, whereas for the triple-layer PRS antenna, the gain bandwidth increased to 390 MHz. The simulated result of the reference antenna has a gain of 3.9 dB at 5.8 GHz. The single-layer and double-layer PRS antennas of 5×5 array show a gain improvement of 62.92% (10.52 dB) and 64.70% (11.05 dB), respectively. The triple-layer PRS cavity antenna with the 5×5 unit cell PRS array achieves a maximum gain of 13.53 dB compared with other antennas, which is 71.19% of the reference antenna as inferred from Figure 12(d). On measurement, the practical gain is slightly dropped down. The maximum practical gain achieved for the triple-layer PRS antenna is 10.28 dB. The deduction of gain and variation in radiation patterns attributes to assembly tolerances, cable losses, and misalignment during measurement.

Table 2 presents the detailed simulated and measured performance comparison of all the designed antenna configurations. Table 3 explains the performance evaluation of the proposed antenna with few existing multilayer PRS antennas. The advantage of the proposed antenna is simple design and is fabricated on a low-cost readily available FR-4 substrate. The designed antenna is smaller in dimensions and uses lesser number of PRS cells and has improved gain compared with the existing PRS antennas operating at 5.8 GHz. The source radiator is a narrow-band patch antenna, thereby the bandwidth of the resultant antenna is

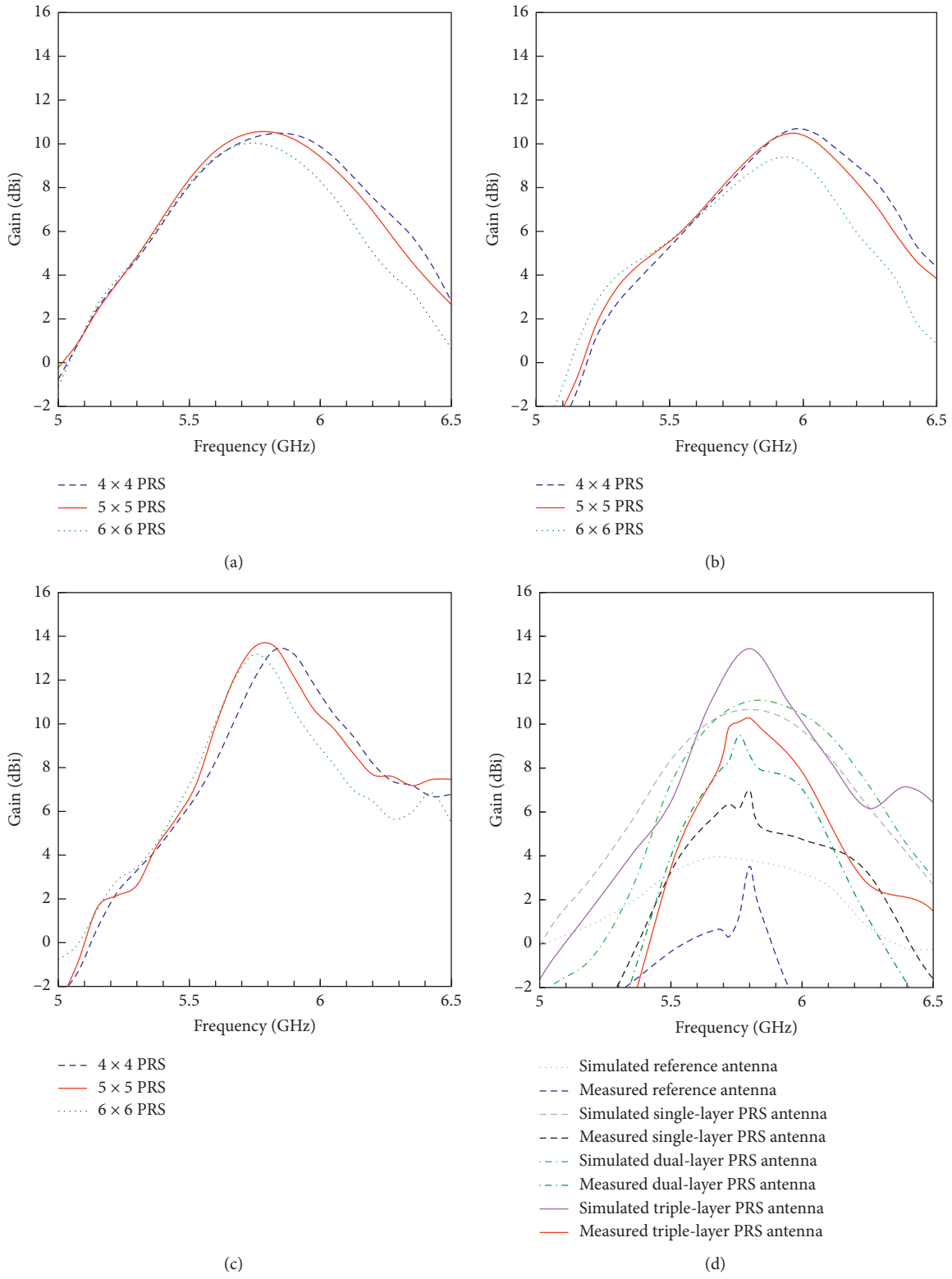

Figure 12: Performance gain comparison of various PRS antenna configurations: (a) simulated single layer, (b) simulated dual layer, (c) simulated triple layer, and (d) simulated and measured 5 × 5 array PRS layers with the reference antenna.

Table 2: Performance comparison of simulated and measured results of the proposed antenna.

Antenna designs	Resonant frequency (GHz)	Return loss (dB)	VSWR	S_{11} bandwidth (MHz)	% S_{11} bandwidth	Gain at 5.8 GHz (dB)	3 dB gain bandwidth (MHz)	% 3 dB gain bandwidth
Simulated antenna results								
Reference	5.8	32.59	1.06	252	4.34	3.9	1038	18.05
Single-layer PRS	5.8	20.37	1.22	346	5.97	10.52	713	12.44
Dual-layer PRS	5.78	33	1.04	263	4.55	11.05	693	11.65
Triple-layer PRS	5.72	24.08	1.13	360	6.29	13.54	365	6.27
Measured antenna results								
Reference	5.755	20.76	1.201	450	7.82	3.52	180	3.1
Single-layer PRS	5.725	17.53	1.306	225	3.93	6.98	640	11.03
Dual-layer PRS	5.725	18.06	1.285	329	5.75	8.6	410	7.09
Triple-layer PRS	5.725	22.123	1.17	205	3.58	10.28	390	6.72

Table 3: Comparison of the proposed antenna with few existing designs.

Reference	Feed antenna	Frequency (GHz)	No of layers	Array size	% S_{11} bandwidth	% 3 dB gain bandwidth	Gain (dBi)	Size (mm^3)
[4]	Slot-coupled patch	16	2	NA	25	25.8	15	$2.5\lambda \times 2.5\lambda \times 1.4\lambda$
[6]	Strip-fed dual-slot	2.4 and 5	2	6×6	16 and 11.7	7 and 11	14.9 and 14.2	$1.3\lambda \times 1.3\lambda \times 0.45\lambda_{2.4GHz}$ $3\lambda \times 3\lambda \times 1\lambda_{5GHz}$
[11]	Aperture slot	80	2	8×4	10	NA	10	$26.5\lambda \times 26.5\lambda \times 1.2\lambda$
[13]	Waveguide slot	14.5	3	5×5	10.3	15	20	$4\lambda \times 4\lambda \times 1.8\lambda$
[15]	Patch	5.8	1	6×6	3.4	NA	9	$2.39\lambda \times 2.39\lambda \times 1.2\lambda$
[16]	CP patch with shorting pin	5.8	1	5×5	NA	2.58	12.9 and 12.8	$3\lambda \times 3\lambda \times 0.55\lambda$
[17]	Patch	13	1	12×12	1.56	8.5	13.6	$3 \times 3 \times 0.65\lambda$
[18]	Aperture-coupled CP patch	4.8	3	6×6	30	29	14.2	$1.6 \times 1.6 \times 0.6\lambda$
[19]	Loop rectangle patch	2.1and5.8	1 (dual-sided)	17×17	NA	NA	6 and4.5	$1.01 \times 1.01 \times 0.09\lambda_{2.1GHz}$ $2.79 \times 2.79 \times 0.27\lambda_{5.8GHz}$
[21]	Dual-slot feed DRA	5.5	2 (dual-sided)	8×8	16	16.4	14.7 and 15.5	$2.1 \times 2.1 \times 0.65\lambda$
[23]	CPMSA	6	2	NA	11.6	14.68	17.4	$2.83 \times 3.23 \times 0.49\lambda$
[27]	Stacked-patch array	13.3	2	9×9	28	31	18	$3.5 \times 3.5 \times 0.53\lambda$
[28]	Strip-fed slot	5	2	4×4	44	45	11.6	$1.1 \times 1.1 \times 0.095\lambda$
[35]	Slot-fed patch array	5.6	1	9×9	7	14.8	7.92	$3.453 \times 3.453 \times 0.5264\lambda$
Proposed	Patch	5.8	3	5×5	6.29	6.7	13.4	$1.65\lambda \times 1.65\lambda \times 1.48\lambda$

*Given antenna dimensions are converted in terms of wavelength for convenience.

reduced. In future, the bandwidth can be enhanced by incorporating metamaterials or frequency-selective surfaces around the feed antenna.

5. Conclusions

In this paper, a novel multilayer PRS unit cell design for dual-band operation is presented. An array of 5×5 PRS unit cells are printed on the FR-4 dielectric substrate and placed above the feed antenna at optimal heights to form single-, double-, and triple-layer PRS cavity antennas. The fabricated triple-layer PRS cavity antenna measured a return loss of 22.12 dB at 5.73 GHz attaining a maximum gain of 65.76%. This achievement is better compared with the existing PRS multilayer antennas with larger number of PRS arrays. The measured S_{11} is in good proximity with the simulated results and is best suited for wireless application. The antenna achieved an impedance bandwidth of 205 MHz and 3 dB gain bandwidth of 390 MHz which is 50% improvement from the reference antenna. The simplified design and low cost make the antenna most suitable for WiMAX applications.

Data Availability

The data used to support the findings of this study are included within the article.

Disclosure

The research was performed as a part of academic interest of the authors and was carried out at PSG College of Technology, Coimbatore, India.

Conflicts of Interest

The authors declare that there are no conflicts of interest regarding the publication of this paper.

Acknowledgments

The authors acknowledge the department of ECE, SSN College of Engineering, for extending their help in antenna measurements.

References

[1] G. V. Trentini, "Partially reflecting sheet arrays," *IRE Transactions on Antennas and Propagation*, vol. 4, no. 4, pp. 666–671, 1956.

[2] Y. Ge, K. P. Esselle, and T. S. Bird, "A method to design dual-band, high-directivity ebg resonator antennas using single-resonant, single-layer partially reflective surfaces," *Progress In Electromagnetics Research C*, vol. 13, pp. 245–257, 2010.

[3] F. Qin, S. Gao, G. Wei et al., "Wideband circularly polarized fabry-perot antenna [antenna applications corner]," *IEEE Antennas and Propagation Magazine*, vol. 57, no. 5, pp. 127–135, 2015.

[4] N. Wang, J. Li, G. Wei, L. Talbi, Q. Zeng, and J. Xu, "Wideband fabry–perot resonator antenna with two layers of dielectric superstrates," *IEEE Antennas and Wireless Propagation Letters*, vol. 14, pp. 229–232, 2015.

[5] C. Chen, Bo-L. Liu, L. Ji, and W.-D. Chen, "A high-isolation dual-polarization substrate-integrated fabry-pérot cavity antenna," *International Journal of Antennas and Propagation*, vol. 2015, Article ID 265962, 6 pages, 2015.

[6] M. L. Abdelghani, H. Attia, and T. A. Denidni, "Dual- and wideband fabry-pérot resonator antenna for WLAN applications," *IEEE Antennas and Wireless Propagation Letters*, vol. 16, pp. 473–476, 2017.

[7] D. Abbou, T. P. Vuong, R. Touhami, F. Ferrero, D. Hamzaoui, and M. C. E. Yagoub, "High-gain wideband partially reflecting surface antenna for 60 GHz systems," *IEEE Antennas and Wireless Propagation Letters*, vol. 16, pp. 2704–2707, 2017.

[8] R. Yahiaoui, T. Beeharry, S. N. Burokur, P. Grassin, and H. H. Ouslimani, "Metasurfaces with positive reflection phase gradients for broadband directive emission," in *Proceedings of the 11th European Conference on Antennas and Propagation (EUCAP)*, pp. 1073–1075, Paris, France, March 2017.

[9] D. B. Brito, G. Adaildo, d'A. ao, H. Robson, C. Manicoba, and X. Begaud, "Metamaterial inspired Fabry–Perot antenna with cascaded frequency selective surfaces," *Microwave and Optical Technology Letters*, vol. 55, no. 5, pp. 981–985, 2013.

[10] C. Mateo-Segura, A. P. Feresidis, and G. Goussetis, "Bandwidth enhancement of 2-D leaky-wave antennas with double-layer periodic surfaces," *IEEE Transactions on Antennas and Propagation*, vol. 62, no. 2, pp. 586–593, 2014.

[11] M. FanHong, H. H. Ouslimani, M. B. Gueye, and Y. Letestu, "Experimental study of 80 GHz Fabry-Pérot cavity antenna based on dual-layer partially reflected surface," *Electronics Letters*, vol. 51, no. 22, pp. 1730–1732, 2015.

[12] A. Hosseini, F. Capolino, and D. R. Jackson, "Leaky-wave explanation of gain-bandwidth-enhanced Fabry-Pérot cavity antennas formed by a thick multilayer partially-reflective surface," in *Proceedings of the IEEE International Symposium on Antennas and Propagation & USNC/URSI National Radio Science Meeting*, Vancouver, BC, Canada, July 2015.

[13] K. Konstantinidis, A. P. Feresidis, and P. S. Hall, "Multilayer partially reflective surfaces for broadband Fabry-Perot cavity antennas," *IEEE Transactions on Antennas and Propagation*, vol. 62, no. 7, pp. 3474–3481, 2014.

[14] K. Konstantinidis, A. P. Feresidis, and P. S. Hall, "Broadband sub-wavelength profile high-gain antennas based on multi-layer metasurfaces," *IEEE Transactions on Antennas and Propagation*, vol. 63, no. 1, pp. 423–427, 2015.

[15] M. A. El Cafsi, L. Osman, A. Gharsallah, M. Nedil, and A. Djaiz, "Multi-layer switched beam Fabry Perot leaky wave antenna," in *Proceedings of the IEEE International Symposium on Antennas and Propagation & USNC/URSI National Radio Science Meeting*, Vancouver, BC, Canada, July 2015.

[16] A. R. Vaidya, R. K. Gupta, S. K. Mishra, and J. Mukherjee, "Right-hand/left-hand circularly polarized high-gain antennas using partially reflective surfacesflective surfaces," *IEEE Antennas and Wireless Propagation Letters*, vol. 13, pp. 431–434, 2014.

[17] H.-Y. Yuan, S.-B. Qu, J.-Q. Zhang et al., "A metamaterial-inspired wideband high-gain fabry–perot resonator microstrip patch antenna," *Microwave and Optical Technology Letters*, vol. 58, no. 7, pp. 1675–1678, 2016.

[18] B. P. Chacko, G. Augustin, and T. A. Denidni, "FPC Antennas: C-band point-to-point communication systems," *IEEE Antennas and Propagation Magazine*, vol. 58, no. 1, pp. 56–64, 2016.

[19] J.-G. Lee and J.-H. Lee, "Low-profile dual-band superstrate antenna using metasurfacefile dual-band superstrate antenna using metasurface," *Progress in Electromagnetics Research C*, vol. 77, pp. 175–184, 2017.

[20] A. Chaabane, F. Djahli, H. Attia, L. Mohamed Abdelghani, and T. Ahmed Denidni, "Wideband and high-gain EBG resonator antenna based on dual layer PRS," *Microwave and Optical Technology Letters*, vol. 59, no. 1, pp. 98–101, 2017.

[21] P.-Y. Qin, Lu-Y. Ji, S.-L. Chen, and Y. Jay Guo, "Dual-polarized wideband fabry-perot antenna with quad-layer partially reflective surface," *IEEE Antennas and Wireless Propagation Letters*, vol. 17, no. 4, pp. 551–554, 2018.

[22] N. N. Trong, H. H. Tran, T. K. Nguyen, and A. A. Abbosh, "Wideband Fabry-Perot antennas employing multilayer of closely spaced thin dielectric slabs," *IEEE Antennas and Wireless Propagation Letters*, vol. 17, no. 7, pp. 1354–1358, 2018.

[23] S. D. Jagtap, R. K. Gupta, N. Chaskar, S. U. Kharche, and R. Thakare, "Gain and bandwidth enhancement of circularly polarized MSA using PRS and AMC layers," *Progress in Electromagnetics Research C*, vol. 87, pp. 107–118, 2018.

[24] M. Wasif Niazn, Y. Yin, S. Zheng, and Z. Zhao, "Dual-polarized low sidelobe Fabry-Perot antenna using tapered partially reflective surface," *International Journal of RF & Microwave Computer Aided Engineering*, Article ID e22070, 2019.

[25] S. Das and S. Sahu, "Design of high gain, broadband resonant cavity antenna with meta-material inspired superstrate," *AEU—International Journal of Electronics and Communications*, vol. 100, pp. 39–46, 2019.

[26] K. Srivastava, A. Kumar, P. Chaudhary et al., "Wideband and high-gain circularly polarized microstrip antenna design using sandwiched metasurfaces and partially reflecting surface," *IET Microwaves, Antennas & Propagation*, vol. 13, no. 3, pp. 305–312, 2019.

[27] L. Asadpor, G. Sharifi, and M. Rezvani, "Design of a high-gain wideband antenna using double-layer metasurface," *Microwave and Optical Technology Letters*, vol. 61, no. 4, pp. 1004–1010, 2019.

[28] Z.-Z. Yang, F. Liang, Yi Yu, D. Zhao, and B.-Z. Wang, "A metasurface-based wideband, low-profile, and high gain antenna," *IET Microwaves, Antennas & Propagation*, vol. 13, no. 4, pp. 436–441, 2019.

[29] Y. Azizi, N. Komjani, and M. Karimipour, "Design and fabrication of a high gain, low cost, LHCP Fabry-Perot antenna at Ku band," *Microwave and Optical Technology Letters*, vol. 61, no. 1, pp. 101–106, 2019.

[30] L. Zhang and T. Dong, "Low RCS and high-gain CP microstrip antenna using SA-MS," *Electronics Letters*, vol. 53, no. 6, pp. 375-376, 2017.

[31] H. Jiang, Z. Xue, M. Leng, W. Li, and W. Ren, "Wideband partially reflecting surface antenna with broadband RCS reduction," *IET Microwaves, Antennas & Propagation*, vol. 12, no. 6, pp. 941–946, 2018.

[32] M. Long, W. Jiang, and S. Gong, "RCS reduction and gain enhancement based on holographic metasurface and PRS," *IET Microwaves, Antennas & Propagation*, vol. 12, no. 6, pp. 931–936, 2018.

[33] T. Debogovic, J. P. Carrier, and J. Bartolic, "partially reflective surface antenna with dynamic beamwidth control," *IEEE Antennas and Wireless Propagation Letters*, vol. 9, pp. 1156–1160, 2010.

[34] B. Ratni, W. A. Merzouk, A. de Lustrac, S. Villers, G.-P. Piau, and S. N. Burokur, "Design of phase-modulated metasurfaces for beam steering in fabry-perot cavity antennas," *IEEE Antennas and Wireless Propagation Letters*, vol. 16, pp. 1401–1404, 2017.

[35] Y. Jia, Y. Liu, X. Yang, Xu Yang, and L. Sun, "A two-dimensional beam tilted Fabry-Perot antenna based on a phase gradient partially reflecting surface," *Microwave and Optical Technology Letters*, vol. 62, no. 2, pp. 887–892, 2020.

[36] P. R. Prajapati and S. B. Khant, "Gain enhancement of UWB antenna using partially reflective surface," *International Journal of Microwave and Wireless Technologies*, vol. 10, no. 7, pp. 835–842, 2018.

[37] H. H. Tran, T. T. Le, C. D. Bui, and T. K. Nguyen, "Broadband circularly polarized Fabry-Perot antenna utilizing Archimedean spiral radiator and multi-layer partially reflecting surface," *International Journal of RF and Microwave Computer Aided Engineering*, vol. 29, no. 3, Article ID e21647, 2019.